UCSF
UC San Francisco Previously Published Works

Title

(19)F-MRI for monitoring human NK cells in vivo.

Permalink

https://escholarship.org/uc/item/50s2n46k

Journal

OncoImmunology, 5(5)

ISSN

2162-4011

Authors

Bouchlaka, Myriam
Ludwig, Kai
Gordon, Jeremy
et al.

Publication Date

2016-05-01

DOI

10.1080/2162402X.2016.1143996

Peer reviewed

eScholarship.org Powered by the California Digital Library
University of California

ONCOIMMUNOLOGY
2016, VOL. 5, NO. 5, e1143996 (12 pages)
http://dx.doi.org/10.1080/2162402X.2016.1143996

Taylor & Francis
Taylor & Francis Group

ORIGINAL RESEARCH

^{19}F-MRI for monitoring human NK cells *in vivo*

Myriam N. Bouchlaka[a], Kai D. Ludwig[b], Jeremy W. Gordon[b], Matthew P. Kutz[a], Bryan P. Bednarz[b], Sean B. Fain[b,c,d], and Christian M. Capitini[a]

[a]Department of Pediatrics, Carbone Cancer Center, University of Wisconsin School of Medicine and Public Health, Madison, WI, USA; [b]Department of Medical Physics, Carbone Cancer Center, University of Wisconsin School of Medicine and Public Health, Madison, WI, USA; [c]Department of Radiology, Carbone Cancer Center, University of Wisconsin School of Medicine and Public Health, Madison, WI, USA; [d]Department of Biomedical Engineering, Carbone Cancer Center, University of Wisconsin School of Medicine and Public Health, Madison, WI, USA

ABSTRACT

The availability of clinical-grade cytokines and artificial antigen-presenting cells has accelerated interest in using natural killer (NK) cells as adoptive cellular therapy (ACT) for cancer. One of the technological shortcomings of translating therapies from animal models to clinical application is the inability to effectively and non-invasively track these cells after infusion in patients. We have optimized the nonradioactive isotope fluorine-19 (^{19}F) as a means to label and track NK cells in preclinical models using magnetic resonance imaging (MRI). Human NK cells were expanded with interleukin (IL)-2 and labeled *in vitro* with increasing concentrations of ^{19}F. Doses as low as 2 mg/mL ^{19}F were detected by MRI. NK cell viability was only decreased at 8 mg/mL ^{19}F. No effects on NK cell cytotoxicity against K562 leukemia cells were observed with 2, 4 or 8 mg/mL ^{19}F. Higher doses of ^{19}F, 4 mg/mL and 8 mg/mL, led to an improved ^{19}F signal by MRI with 3×10^{11} ^{19}F atoms per NK cell. The 4 mg/mL ^{19}F labeling had no effect on NK cell function via secretion of granzyme B or interferon gamma (IFNγ), compared to NK cells exposed to vehicle alone. ^{19}F-labeled NK cells were detectable immediately by MRI after intratumoral injection in NSG mice and up to day 8. When ^{19}F-labeled NK cells were injected subcutaneously, we observed a loss of signal through time at the site of injection suggesting NK cell migration to distant organs. The ^{19}F perfluorocarbon is a safe and effective reagent for monitoring the persistence and trafficking of NK cell infusions *in vivo*, and may have potential for developing novel imaging techniques to monitor ACT for cancer.

ARTICLE HISTORY
Received 2 October 2015
Revised 11 January 2016
Accepted 13 January 2016

KEYWORDS
Fluorine 19 (^{19}F); *in vivo* imaging and adoptive cell therapy (ACT); magnetic resonance imaging (MRI); natural killer cells (NKs)

Introduction

The infusion of NK cells as treatment for relapsed solid tumors has been utilized by many centers based on emerging preclinical evidence of antitumor activity. Melanoma, renal cell carcinoma, recurrent breast and ovarian cancer have been treated with NK cells or NK cell lines in adults,[1-5] while neuroblastoma, medulloblastoma, osteosarcoma, rhabdomyosarcoma and Ewing sarcoma are being tested in children.[6] As NK cells are being more widely used for cancer treatment, understanding where adoptively transferred NK cells traffic after infusion is becoming more critical. It is also not known how long adoptively transferred NK cells persist *in vivo*, making timing of repeated NK cell infusions difficult to predict. According to the Food and Drug Administration (FDA) Cellular, Tissue and Gene Therapy Advisory Committee, there is an urgent need to track cells *in vivo* to determine migration patterns and longevity.[7] A thorough summary of imaging methods that have been employed to track NK cells has been reviewed previously.[8,9] Usage of superparamagnetic iron oxide (SPIO) particles have been previously used to label NK cell lines[10-13] for detection in preclinical models by MRI, but have not gained wider clinical use. One limitation is that the hypointense signal produced can make it difficult to discriminate the SPIO-labeled cells from other hypointense signals, like blood, or from signal loss due to susceptibility and field inhomogeneities. ^{19}F is a nonradioactive, 100% naturally abundant isotope of fluorine that can be formulated into perfluorocarbon nanoemulsions and simply incubated with cells in culture.[14] Radiofrequency MRI coils can then be tuned to detect and image these fluorine atoms enabling tracking of cellular fate post-infusion.[15]

In preclinical models, optical imaging using fluorescent and bioluminescent models have provided valuable insight into NK cell trafficking patterns after adoptive transfer,[16-18] but these techniques assume murine NK cells traffic similarly to human NK cells, do not give high resolution of the live gross anatomical structures where the NK cells traffic to, and most importantly, are not available in the clinic. Radiolabeling of NK cells with clinically available isotopes, like ^{18}F, ^{11}C or ^{111}In, offers high sensitivity but also lacks high resolution of anatomical structures, exposes the patient to ionizing radiation, and is limited by radioactive decay of the isotope (typically hours to days) preventing detection of long-term NK cell persistence. Plus, the FDA's Center for Devices and Radiological Health has launched an initiative to reduce unnecessary radiation exposure from medical imaging.[19]

In the past decade, very promising MRI techniques have been developed to monitor and quantify immune cells *in vivo* using the non-radioactive nucleus ^{19}F as an MRI contrast agent.[14,20,21] Because there are trace amounts of fluorine in the body (mainly in the bone matrix and teeth) that exhibit a very

CONTACT Christian M. Capitini ccapitini@pediatrics.wisc.edu
© 2016 Taylor & Francis Group, LLC

short spin–spin relaxation time,[15] there is minimal background "noise" and infusions of ^{19}F-labeled cells could be easily identified at a high contrast to noise ratio.[22] With a high gyromagnetic ratio similar to that of ^{1}H, ^{19}F has favorable physical properties that improve inherent receptivity and sensitivity, requiring only millimolar quantities per voxel for detection.[22] Furthermore, ^{19}F is non-radioactive, non-invasive; depth independent since used by MRI and has no known enzyme for its degradation *in vivo* (cleared by exhalation or by endoreticulum). Moreover, perfluorocarbon liquids are chemically and biologically inert, and no toxicity has ever been reported using ^{19}F-labeled cells,[23] even at large doses. To date, investigators have successfully used this approach to track murine macrophages,[24] murine[14] and human dendritic cells,[25,26] murine T cells,[27,28] hematopoietic,[29] both murine[30] and human neural stem cells[31] as wells as murine[32] and human mesenchymal stem cells[33] in preclinical models. Interestingly, ^{19}F has been FDA approved in a phase I clinical trial to monitor a DC vaccine in colorectal patients. Initial results from three patients have recently been published showing the ability to detect human DCs by ^{19}F-MRI without apparent toxicity.[34] However, NK cells have been challenging to label using this approach[35] and data is lacking on NK cell trafficking even though they are being infused in clinical trials.

In this study, we will show the impact of labeling human NK cells with a commercially available ^{19}F perfluoropolyether (PFPE) nanoemulsion on viability, cytotoxicity and cell surface marker expression on *in vitro* human NK cell cultures. We will also show that MRI can detect ^{19}F-labeled human NK cells after subcutaneous and intratumoral injection. Our preliminary results indicate that^{19}F MRI is a promising approach for tracking NK cells *in vivo* noninvasively without toxicity or ionizing radiation, and has sufficient resolution to detect NK cells within a solid tumor.

Results

Labeling of human NK cells with ^{19}F

We first determined the impact of labeling IL-2 expanded NK cells *ex vivo* with ^{19}F by analyzing NK cell viability with increasing concentrations of the tracer. We found no impact on cell viability after 24 h incubation with 2 or 4 mg/mL ^{19}F, compared to unlabeled NK cells (Fig. 1A). Viability of NK cells was only decreased at 8 mg/mL ^{19}F (Fig. 1A). Using NMR, we detected up to 3.78×10^{11} atoms of ^{19}F per NK cell on average, which plateaued between labeling with 4 to 8 mg/mL ^{19}F (Fig. 1B–C). Based on the similar efficiency of internalization of ^{19}F using 4 mg/mL or 8 mg/mL, and since NK cell viability is decreased with 8 mg/mL ^{19}F, we decided to use 4mg/mL ^{19}F for all subsequent experiments.

NK cell receptor expression upon ^{19}F labeling

We then evaluated the effects of ^{19}F labeling on $CD3^{-}CD56^{+}$ NK cell surface receptors expression, particularly those that are involved in NK cell antitumor activity. There were no differences in natural cytotoxicity receptor (NCR) expression in NKp30, NKp46 and NKp44 expression between unlabeled and ^{19}F-labeled NK cells for 24 h (Fig. 2A–B). Additionally, no changes were noted in the activating receptors DNAM-1 or NKG2D and in CX3CR1 and CXCR4 chemokine receptor expression both in percentages (Fig. 2C–E) and in mean fluorescent intensity (MFI) (Fig. 2F–G). NKG2D ligands include MHC class-I-related protein and stress molecules that are upregulated upon DNA damage and heat shock responses in malignant transformations. On the other hand, DNAM-1 receptor, a member of the immunoglobulin superfamily, binds to poliovirus receptor CD155 and CD112 (Nectin-2), both ligands are expressed on some tumor cells. Furthermore, DNAM-1 has been shown to be important in the clearance of tumor cells that lack the expression of ligands to NK-activating receptors.[36] Therefore, ^{19}F labeling of NK cells does not appear to affect surface expression of NCRs, receptors to stress ligands, and chemokine receptors suggesting that NK cell migration ability and immunosurveillance against tumors should remain preserved.

In vitro cytotoxicity of ^{19}F-labeled NK cells

While our flow cytometry data demonstrates that ^{19}F does not negatively impact the expression of NK cell cytotoxicity receptors, we next tested the impact of ^{19}F labeling on NK cell tumor cytotoxicity against K562 cells. There were no differences in NK cell cytotoxicity between unlabeled and NK cells labeled with 2 mg/mL, 4 mg/mL or 8 mg/mL ^{19}F PFPE (Fig. 3A). We next evaluated NK cell function after *in vitro* stimulation by measuring intracellular production of IFNγ and granzyme B, which are both essential mediators in tumor lysis. By comparing unlabeled versus ^{19}F-labeled NK cells, we found no difference in granzyme B production in percentage and MFI (Fig. 3B–D), whereas a mild increase in the percent and MFI of NK cells secreting IFNγ was observed in ^{19}F-labeled NK cells (Fig. 3B–D). To verify this observation, we quantified IFNγ secretion by ELISA and found no differences after 24 or 48 h of ^{19}F labeling at both 2 mg/mL and 4 mg/mL concentrations (Fig. 3E). Preservation of NK cell production of granzyme B and IFNγ after ^{19}F uptake correlates with their *in vitro* ability to mediate antitumor responses.

In vivo detection of ^{19}F-labeled NK cells by MRI

Next, we wanted to examine if ^{19}F-labeled NK cells could be detected by *in vivo* MRI using a volumetric ^{1}H/^{19}F quadrature coil. We performed intratumoral injection of ^{19}F-labeled NK cells into two different xenograft tumor models to determine if the NK cells could be detected within a bulky tumor mass. NK cells were detected at both 1 hour and 48 h after injection into immunodeficient mice bearing human neuroblastoma (Fig. 4A) as well as up to 8 d after injection into human lymphoma (Fig. 4C). On day 0, quantification of ^{19}F signal from the NK cells using MRI showed detection of 95% of the NK cells injected intratumor for the neuroblastoma and 84% NK cells detected after 48 h (Fig. 4B). However, only 74% of the NK cells were detected on day 0 for the lymphoma-bearing mouse and the number of NK cells detected by day 8 was 68% (Fig. 4D). Overall, very little to no migration of the NK cells out of the tumor was observed and a high number of NK cells could be detected within a bulky tumor mass over the duration of the experiment (Fig. 4).

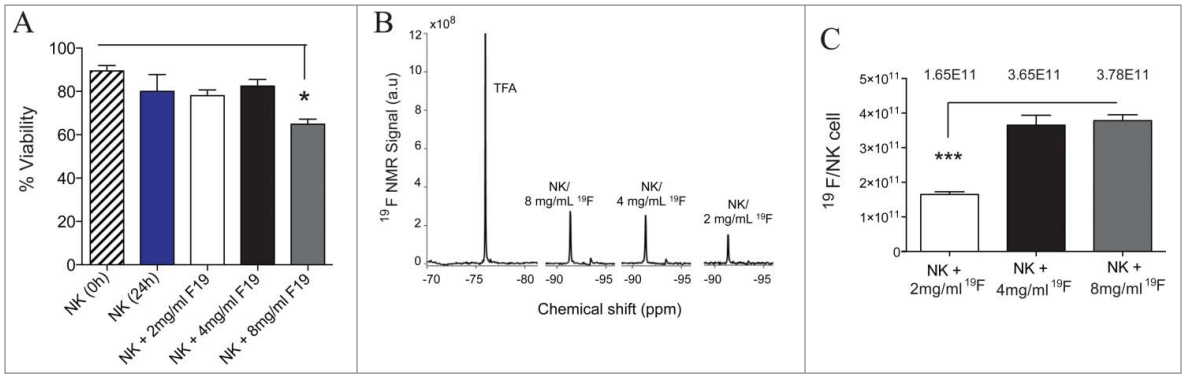

Figure 1. High uptake of ^{19}F nanoemulsions by human NK cells do not affect their viability. Human NK cells were expanded for 12 d from PBMCs of a healthy donor and sorted on day 12 of expansion by magnetic bead isolation. Sorted NK cells ($CD3^-$ $CD56^+$) were co-incubated with or without ^{19}F (Cell Sense) for 24 h then analyzed for (A) Percent viability using Trypan blue and determined before (0 hour) and after (24 h) co-culture of NK cells with 2 mg/mL, 4 mg/mL or 8 mg/mL ^{19}F. Data presented for 11 compiled experiments. (B) Representative NMR spectra of TFA (control) or NK cells labeled with 2 mg/mL, 4 mg/mL or 8 mg/mL PFPE show ^{19}F signal increasing with the concentration of PFPE in cell media. (C) Concentration of ^{19}F/NK cell determined by NMR for NK cells exposed to different concentration of PFPE for 24 h. Three replicates were set up per group. Bar graph values represent the mean ± SEM tested by a one-way ANOVA. Data representative of at least three experiments with reproducible results.

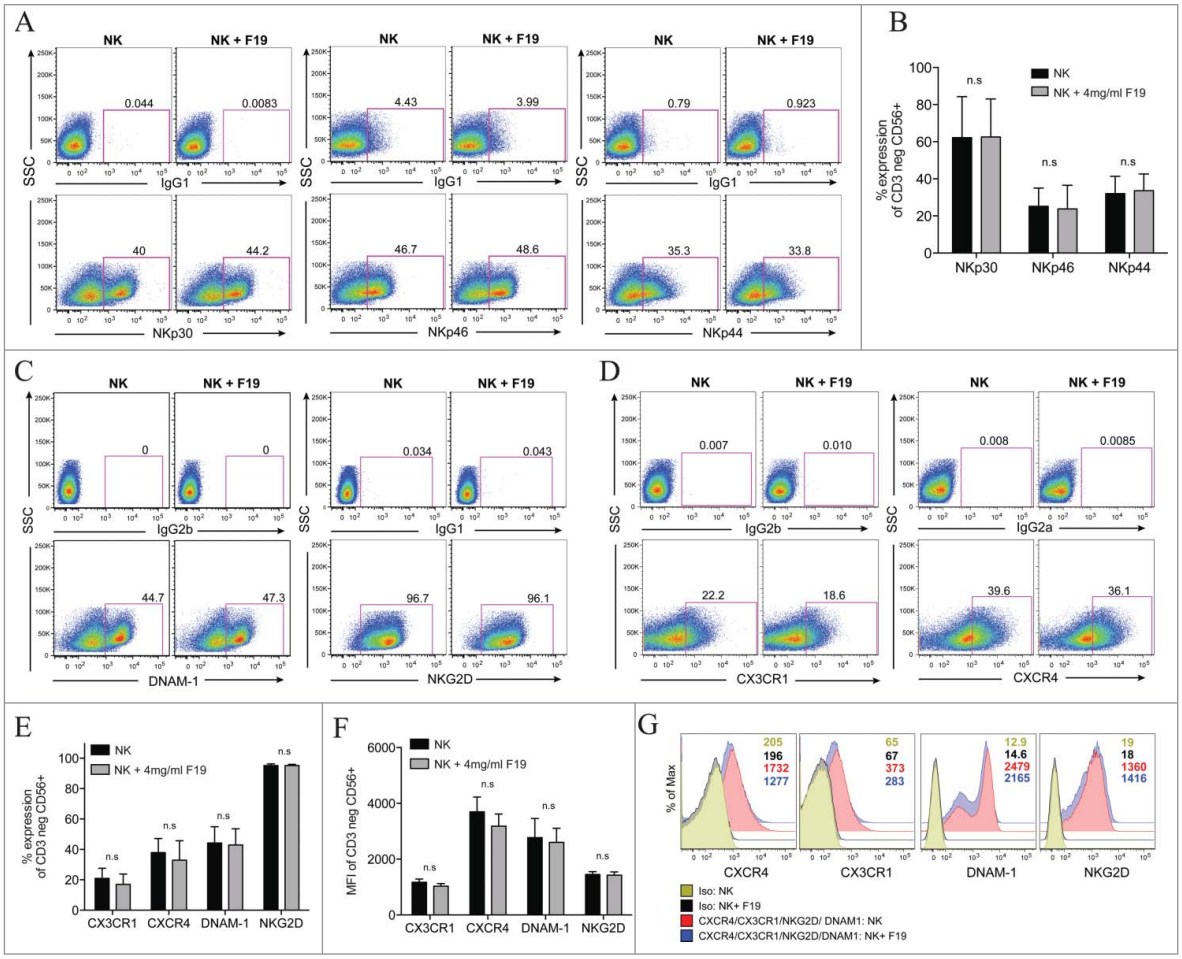

Figure 2. ^{19}F labeling of human NK cells does not alter their surface expression of activating natural cytotoxic receptors and chemokine receptors. (A–G) Human NK cells unlabeled or labeled with 4 mg/mL ^{19}F (Cell Sense) for 24 h analyzed by flow cytometry for: (A–B) The percent expression in the NK cytotoxic receptors (NCRs) NKp30, NKp46 and NKp44 vs. IgG1 control stains. (A) Illustrates representative dot plots for each NCR and their isotype controls (IgG1) for unlabeled NK cells or NK cells labeled with ^{19}F. (B) Shows percentage of NKp30, NKp46 and NKp44 on the NK cells (CD3 negative $CD56^+$) in five healthy donors. (C–E) The percent expression or (F–G) mean fluorescent intensity (MFI) in the activating receptors DNAM-1 (DNAX Accessory Molecule-1) and NKG2D and in chemokine receptors CX3CR1 and CXCR4 compared to isotype controls in ^{19}F-labeled or unlabeled NK cells. (D) Percent expression or (G) MFI in the chemokine receptors CX3CR1, CXCR4 or isotype controls after gating on the of CD3neg $CD56^+$ NK cells. MFI numbers are indicated within the histograms with color-coded MFIs indicated in the legend and corresponding to the histograms. (E) Shows the percent and (F) MFI in CX3CR1, CXCR4, DNAM-1 and NKG2D on NK cells from five healthy donors labeled or not with ^{19}F. All gates and histograms are pre-gated on $CD3^-$ $CD56^+$ NK cells. Bar graph values represent the mean ± SEM tested by two-way ANOVA. Data representative of at least four independent experiments with reproducible results. n.s.= not significant.

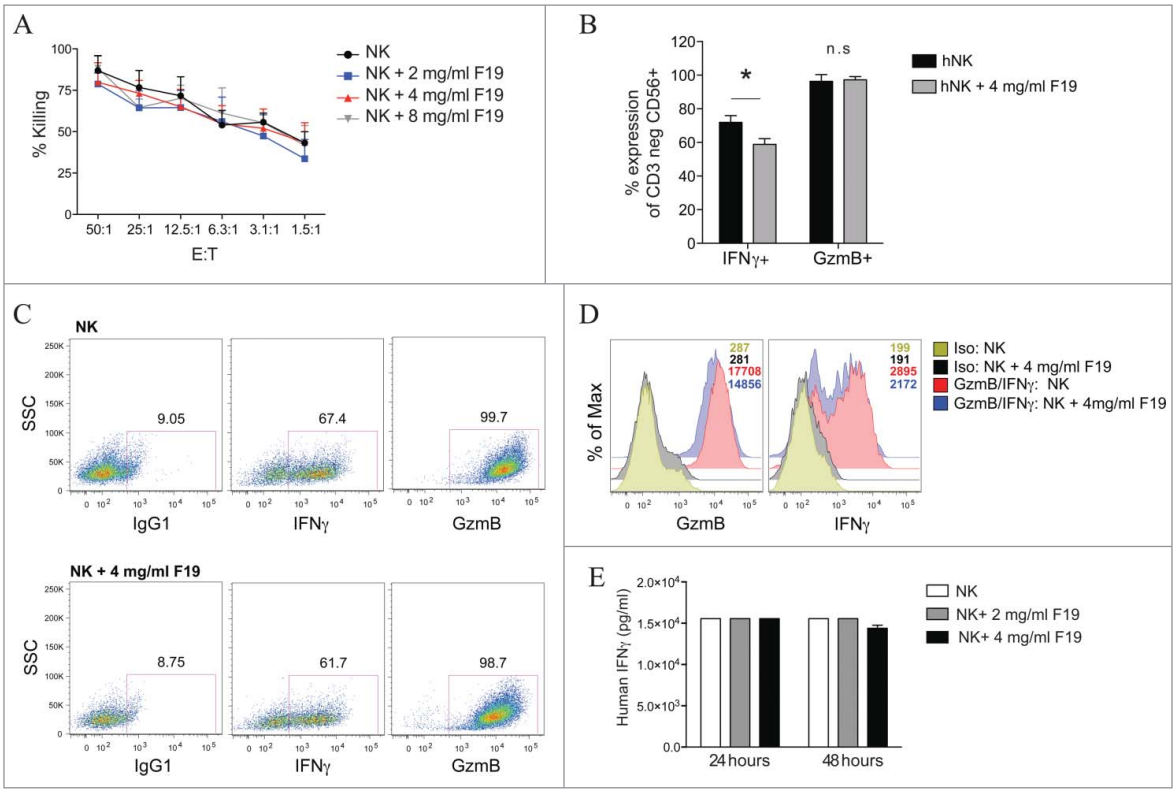

Figure 3. Human NK cells labeled with ^{19}F maintain their cytotoxic function *in vitro*. (A) Sorted human NK cells were cultured with ^{19}F for 24 h. Extra ^{19}F not taken up by NK cells was washed out, then NK cells (E: effectors) were cultured with ^{51}Cr-labeled K562 tumor (T: target) for 4 h at 37°C at different E:T ratios to determine their percent lysis of tumor cells, n = 5. Values represent the mean ± SEM of one of four independent experiments tested by two-way ANOVA, with no significant difference seen. (B–D) NK cells labeled with 4 mg/mL ^{19}F or unlabeled were stained for flow cytometry intracellularly for IFNγ and granzyme B or isotype control, n = 5 donors. (B) Compiled percentage or (C) representative flow plots or (D) MFI in isotype control, IFNγ and Granzyme B by unlabeled and ^{19}F-labeled NK cells is illustrated. (E) Human IFNγ production was determined by ELISA in NK cells unlabeled or labeled with ^{19}F at 2 mg/mL or 4 mg/mL ^{19}F for 24 h or 48 h, n = 3, no difference was observed. Dot plots are representative of one of at least five experiments with reproducible results. Bar graph values represent the mean ± SEM of one of five independent experiments tested by two-way ANOVA. $p < 0.05$, n.s = not significant.

Migration of ^{19}F-labeled NK cells in vivo

Finally, we sought to determine the ability of ^{19}F-labeled NK cells to migrate to a distant tumor. To address this, ^{19}F-labeled NK cells were injected subcutaneously into the contralateral flank of mice bearing human melanoma (M21). In order to aid in the migration of NK cells to the tumor site, the hu14.18-IL-2 immunocytokine was injected intratumorally (50 ug/50 uL) on days 0–2 and 7–9 post NK cell infusion in addition to intraperitoneal injection of recombinant human IL-2 (1×10^6 IU/0.2 mL) on days 0 and 7 post NK cell infusion. M21 tumors express the disialoganglioside GD2, while the hu14.18-IL18 immunocytokine consists of a GD2-specific monoclonal antibody (mAB) fused to human IL-2 able to recognize and specifically bind to GD2$^+$ tumors. The immunocytokine has shown antitumor effects *in vivo* in mouse models[37-40] in a phase I/II clinical trial in pediatric patients with relapsed/refractory neuroblastoma[41,42] and in patients with metastatic melanoma.[43] Therefore, we expected that GD2$^+$ tumor and the treatment with hu.14.18-IL2 would recruit NK cells to mediate ADCC at the tumor. At day 0, 10×10^6 ^{19}F-NK cells were implanted subcutaneously (flank opposite to the tumor) with on average 9.1×10^6 NK cells detected by MRI on day 0 (Fig. 5A–B). Over time we observed a progressive decease in ^{19}F signal from the NK cells with about 65% of the NK cells or ^{19}F signal remaining at the site of injection by day 15 (Figs. 5A–B). The decrease in ^{19}F signal is indicative of the migration of the NK cells out of the inoculation site to distant organs. However, the ^{19}F signal from the NK cells was not detected at the tumor site or at other organs by MRI (Fig. 5A).

Discussion

Infusions of NK cells for cancer immunotherapy represent an evolving approach both for solid and hematologic cancers and are already occurring at centers around the world.[44] Above all, few toxicities have been reported following adoptive transfer of NK cells. However, very little is known about the migration, persistence and biodistribution of NK cells post infusion. In this paper, we show for the first time that ex vivo expanded human NK cells can be efficiently labeled with ^{19}F, enabling their *in vivo* detection and quantitation by MRI in immunodeficient mice and within the dense architecture of a solid tumor. Importantly, ^{19}F labeling of human NK cells does not alter their viability, their expression of NCRs, cytokines and granzymes necessary for their cytotoxic functions.

Although NK cells have shown antitumor effects in preclinical models, their full therapeutic potential in the clinic has yet to be optimized. Typically, efficacy of cellular therapy is evaluated on the basis of survival rate and tumor regression assessed for weeks and months post treatment. However, lack of response cannot be positively attributed to the inefficacy of NK

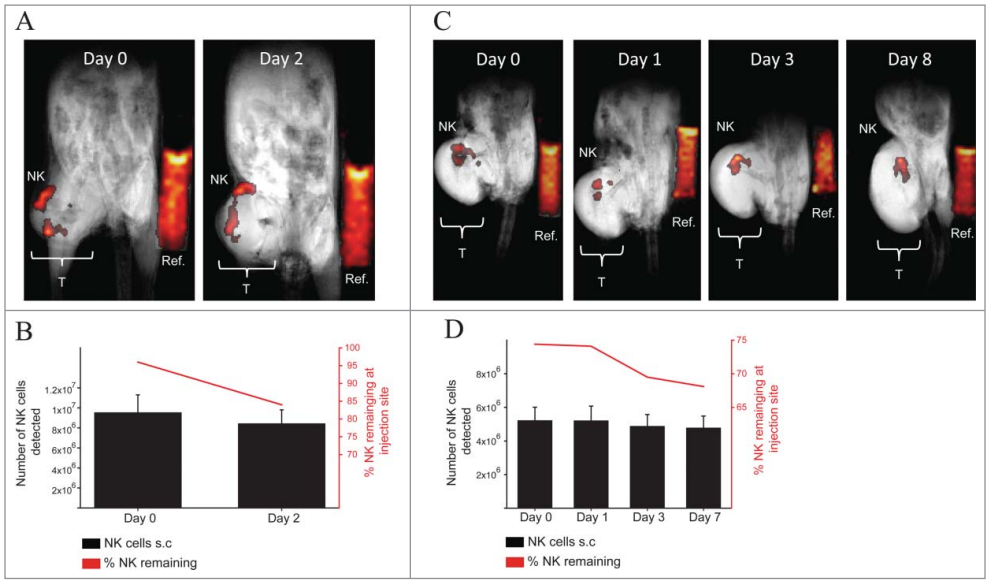

Figure 4. MRI *in vivo* detection of ^{19}F-labeled human NK cells in NSG mice bearing xenograft human tumors. (A–B) 10 × 10^6 ^{19}F-labeled (4 mg/mL PFPE for 24 h) human NK cells were injected intratumor into one NSG mouse bearing a human neuroblastoma (CHLA-20) on the right flank (T: Tumor). ^{19}F intensity from NK cells or from the reference (Ref: Reference vial of ^{19}F) vial is displayed on a "hot-iron" scale. Mouse was imaged for ^{1}H and ^{19}F by MRI using a volumetric coil and anesthetized using ketamine and xylazine. (A) Composite ^{19}F/^{1}H images at 0 or 2 d post NK cell injection are shown with 32 min and 42 min of scan time for each day respectively. (B) The number (black bars corresponds to left y-axis) and percentage (red line graph corresponds to the right y-axis) of NK detected in the tumor is denoted and was determined based on the efficiency of ^{19}F uptake by NK cells from NMR analysis. (C–D) 7 × 10^6 ^{19}F-labeled (4 mg/mL PFPE for 24 h) NK cells were injected intratumor into one NSG mouse bearing a human mantle cell lymphoma (Z138) on the right flank. (C) Imaging for ^{1}H and ^{19}F was established as described in (A) with scan time of 42 min for each time point. (D) Number (black bars corresponds to left y-axis) and percentage (red line graph corresponds to the right y-axis) of NK cells detected at the tumor site is denoted for each imaging time point. Values represent the mean ± SEM of one single experiment. The uncertainty in the ^{19}F reference mean signal ($\sigma_{\bar{S}_R}$) was estimated as the standard deviation of the ROI drawn on the reference (see methods for quantification of ^{19}F signal).

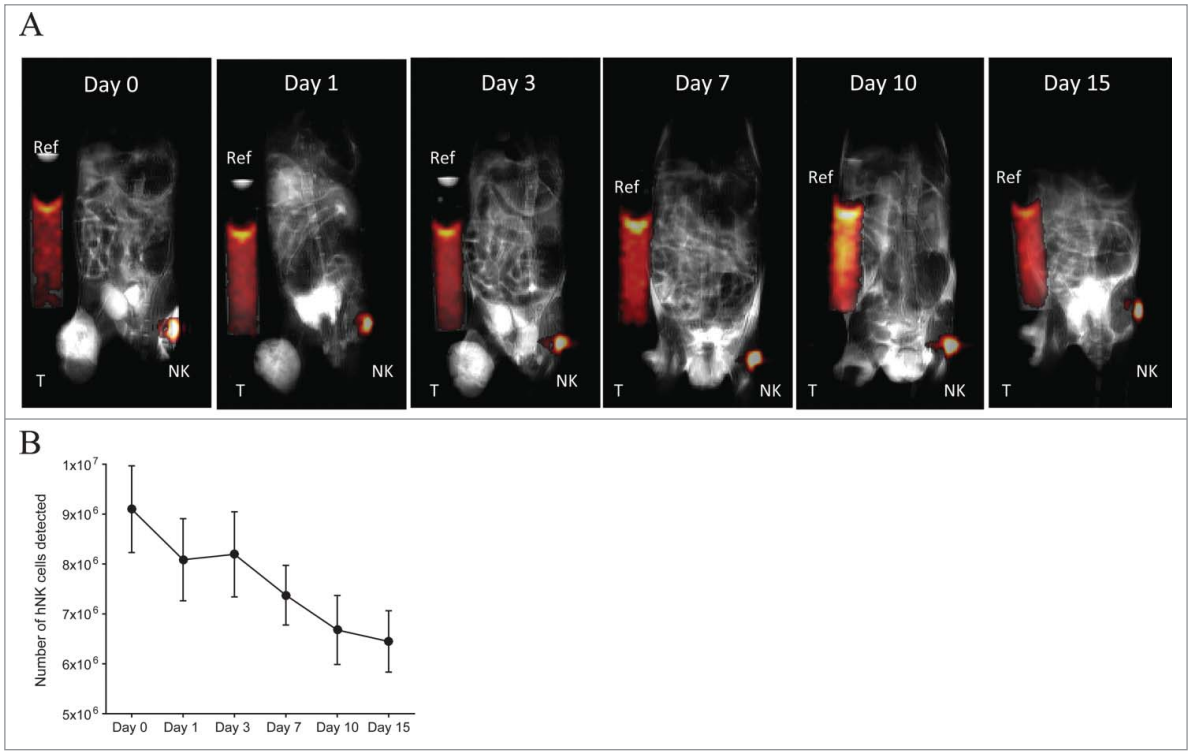

Figure 5. ^{19}F-labeled NK cell migration in NSG mice bearing human GD2$^+$ melanoma and hu14.18-IL-2 treatment. 10 × 10^6 ^{19}F-labeled (4 mg/mL PFPE for 24 h) human NK cells were injected on the left flank subcutaneously into NSG mice (n = 2) bearing human melanoma (M21) tumor on the right flank (T: Tumor). On days 0–2 and 7–9, 50 μg/50 μL hu.14.18-IL-2 immunocytokine was injected i.t. On days 0 and 7, 1 × 10^6 IU/0.2 mL rh-IL-2 was injected i.p. (A) Mice were imaged for ^{1}H and ^{19}F by MRI for 42 min at different time points. Here, a T2-weighted ^{1}H image was acquired for enhanced tumor visualization. Composite ^{19}F/^{1}H images are depicted for 1 mouse. (B) Illustrates the number of NK cells remaining at the site of injection at each time point for both mice. Day 0 refers to the day of implantation of ^{19}F-labeled human NK cells. Values represent the mean ± SEM of one single experiment, n = 2.

cells without direct measurement of the location of NK cells in respect to the tumor site and also their persistence post adoptive transfer. The lack of response to NK cell immunotherapy could simply be due to their inability to migrate to the tumor, to a low concentration of transferred NK cells or to a need of multiple adoptive transfers, all of which are dependent on the tumor type (solid vs. blood-borne), the stage of cancer and resistance of the tumor. Presently, we rely on non-specific and insensitive blood draws and bone marrow biopsies to locate infused NK cells by flow cytometry and immunohistochemistry, even though the NK cells may be in secondary lymphoid tissues or in the tumor. Moreover, biopsy of tumors is a difficult and invasive procedure that may lead to the potential of sampling error and risk to the patient. Thus, the field of cellular immunotherapy is in need of a means by which to non-invasively track infused NK cells in both normal organs and tumors.

Usage of ^{19}F is an appealing labeling approach for *in vivo* imaging of NK cells (or other cell therapies) because (1) it is the only naturally occurring isotope of fluorine and does not decay, (2) does not require phagocytosis to enter the cell, (3) is a component of the chemical structure of over a dozen FDA-approved drugs and thus has a long safety record in humans,[15] and (4) perfluorocarbons have already been successfully used in clinical trials for decades in artificial blood substitutes.[45] Moreover, using ^{19}F-MRI is an attractive technique as it provides positive contrast, and the high-resolution anatomical ^{1}H clinical images can be registered and superimposed with the highly sensitive ^{19}F hotspot images to create a precise mapping of where the ^{19}F-labeled NK cells exist in relation to the patient's tumor. The ability for repeated imaging over time with ^{19}F-MRI will also provide a sense of trafficking patterns as well as NK cell persistence after infusion. Longer lived PET isotopes such as ^{89}Zr have recently been used in combination with more specific cell labeling strategies such as so-called "click chemistry" to enhance signal half-life and specificity with promising results.[46-48] However, prolonged exposure to ionizing radiation remains problematic for cell-trafficking approaches in the clinic.

Perfluorcarbon ^{19}F nanoemulsions have gained interest in the past decade as an imaging modality to *ex vivo* label immune cells and monitor their biodistribution *in vivo* using MRI.[20] Ahrens et al. were first to initially demonstrate the ability to efficiently label murine DCs *ex vivo* with perfluoropolyether (PFPE) agents. In their study, they showed that PFPE does not affect DC function *in vitro* and were able to track DC migration in mice from the foot pad to the popliteal lymph node 6 h post injection.[14] Intravenous injection of PFPE-labeled murine DCs were effectively visualized using an 11.7 Tesla vertical bore MRI and accumulated mainly in the liver and spleen.[14] The same group has subsequently employed ^{19}F-MRI to track and quantify: autoreactive mouse T cells,[27] antigen specific T cells,[28] monocyte and macrophages in two rat models of renal and cardiac allograft rejection,[24] and PFPE-labeled human primary DCs in immunodeficient mice.[25,26] Other investigators have also reported on the ability to *ex vivo* label other potential cell therapies with ^{19}F, including murine[30] and human neural stem cells,[31] human CD34^{+} hematopoietic stem cells (HSCs) and mouse bone marrow derived HSCs as well as murine[32] and human[33] mesenchymal stem cells. All of the aforementioned groups have demonstrated that ^{19}F labeling of immune and non-immune cells does not alter their cell viability, phenotype, proliferation or function *in vitro* compared to unlabeled cells.

Furthermore, Ahrens *et al.* were first to prove the feasibility of labeling human immune cells and monitor their migration in mice, although duration of imaging was reported only for 18 h post injection of the human DCs.[25] This has led to usage of ^{19}F in a phase I clinical trial to monitor an autologous DC vaccine in colorectal patients. Initial results from three patients have recently been published showing the ability to detect human DCs by ^{19}F-MRI without apparent toxicity.[34] About 10 million DCs were injected intradermally into quadriceps and patients were imaged for about 9.5 min. DCs were detected 4 h post inoculation with a 50% decrease in ^{19}F signal at the site of injection by 24 h post inoculation in two patients.[34] These data demonstrate the feasibility to visualize human immune cells using ^{19}F-MRI, however long-term studies in patients are needed to confirm persistence of ^{19}F signal from the adoptively transferred cells, toxicity and potential false positive signal from death of transferred cells leading to transfer of ^{19}F signal to other host cells. To our knowledge no report has applied 19F-MRI to track human NK cells *in vivo*.

Several other imaging techniques have been used in pre-clinical or clinical scenarios to monitor NK cells in recipients and monitor the tumor response. These techniques include positron emission tomography (PET), single photon emission computed tomography (SPECT), and optical imaging (OI) (bioluminescence and fluorescence imaging).[8,9] *In vivo* studies using immunocompetent mice or xenogeneic mouse models, mouse NK cells or human NK cell lines (NK92) have been labeled with the radionuclides ^{18}FDG or ^{11}C-methyl iodide for detection by PET. Allogeneic or autologous human NK cells were also labeled *ex vivo* with the gamma emitting radioisotope indium-111 oxine (^{111}In) for detection by SPECT in patients with renal cell carcinoma[49,50] and in patients with colon cancer with liver metastasis.[51] In the renal cell carcinoma patients, the NK cells initially accumulated to the lungs, after intravenous injection, and redistributed to the liver and metastatic tumors (lungs and livers) within 24 h.[49,50] Conversely, in the study with the colon cancer patients, NK cells were only detected within the tumor after intra-arterial delivery of the NK cells.[51] However, the inability to distinguish from cell-bound versus free ^{111}In might give false positive for the true localization of NK cells.[50]

PET/SPECT imaging provides high sensitivity and specificity, and could be immediately translated to the clinic through the use of FDA-approved radioisotopes (^{18}FDG and ^{111}In). However, several limitations to PET/SPECT still exist. These include mainly ionizing radiation exposure to the patients and fast decay of the tracers ($t_{1/2}$ = 2.8 d for ^{11}In, $t_{1/2}$ = 109 min for ^{18}FDG, and $t_{1/2}$ = 20 min for ^{11}C) which would limit the ability for longitudinal studies to monitor the persistence and biodistribution of the adoptively transferred cells.[9,52] Moreover, these radionuclide-based methods have low anatomical resolution (PET/SPECT) and have to be combined with other modalities such as CT (CT) or MRI, which increases the complexity of the methodology and the costs. Using optical imaging (OI), NK cells or NK cell lines (NK92) can be detected *in vivo* after direct *ex vivo* labeling with organic fluorochromes (i.e., quantum dots,

Cy5.5)[23,53,54] or indirectly via transfection of a reporter gene for bioluminescence imaging (BLI) (i.e., luciferase or green fluorescent protein (GFP)).[55,56] The advantages of OI methods over MRI or PET/SPECT include cheaper cost of instrumentation, fast imaging, and radiation-free imaging. However, OI is also limited by poor resolution (2–3 mm), lower sensitivity in the case of GFP due to auto-fluorescence and toxicity for certain organic fluorochromes (i.e., quantum dots contain cadmium). Importantly, the main disadvantage to optical methods for cell tracking *in vivo* is its limited tissue penetration of light (1 mm for fluorescence; 3 mm for bioluminescence), which restricts its application to only small animal imaging and currently there are no available instrumentation for clinical application of optical imaging.[8,9,52,57]

Compared to PET or OI, MRI is unique as it allows for higher resolution images (100 μm) regardless of tissue depth, does not use ionizing radiation, and allows for high specificity of signal from the transferred cells. However, it is very difficult to generate the contrast necessary to visualize the transplanted cells due to the high ^{1}H background signal from water *in vivo*. Different images acquired before and after the transfer of the labeled cells can improve contrast but are problematic due to variations in the patient's positioning and due to motion. Additionally, if using gadolinium (Gd^{3+}), it has to be chelated to limit its toxicity and has finite stability so may be problematic for extended residence times *in vivo* due to eventual release in tissues as free ion. While MRI offers the most beneficial methodology to track immune cells *in vivo*, conventional contrast agents used clinically do not allow for quantitative and longitudinal assessment of the transferred cells.

Labeling of NK cells with ^{19}F has been reported to be challenging.[35] Our data shows for the first time that ^{19}F labeling of human NK cells is feasible, nontoxic and does not appear to affect viability, cytotoxicity or cytokine secretion by NK cells. We also observed no impact on expression of chemokine or activating receptor involved in NK cell cytotoxicity. Since ^{19}F is passively taken up by NK cells, labeling can be performed in a relatively short period of time (24 to 48 h) at the end of an *ex vivo* expansion, and does not require extensive manipulation of NK cell cultures. Using subcutaneous and intratumoral injection, we were able to detect infused ^{19}F-labeled NK cells *in vivo*. In human tumor bearing mice, we are able to show a loss of ^{19}F-signal from the NK cell injection site, which is indicative of the migration of the NK cells from the primary injection site to distant organs and perhaps to the tumor site. Also for the first time, we show that an immune effector cell can be visualized within a tumor, via intratumoral injection, using ^{19}F-MRI. Intratumoral injection of cytokines and ACT has been used previously as an effective route of cancer immunotherapy,[58,59], and provides "proof of concept" evidence that NK cells can be imaged within a bulky tumor microenvironment.

All previously published data on ^{19}F-MRI imaging of mouse or human immune cells *in vitro* or implanted in xenogeneic mice have used MRI scanners with field of strength ranging between 7.0T and 11.7T with the shortest imaging session of 1.5 h and up to 3 h per animal.[14,25-27,30-32] Conversely, we used a 4.7T MRI scanner with the total imaging session per animal not exceeding 1 h of scan time. The strength of our MRI is closer to the field strength of MRIs in clinical practice today, making our imaging methodology more relevant for clinical imaging of ACT.[34] One obvious limitation of our MRI coil was in the inability to detect ^{19}F-labeled NK cells after intravenous (i.v.) infusion (data not shown), the most common route of therapy. Typically, cells infused i.v. first accumulate in the lungs which has a low water content (and thus low ^{1}H signal) and is difficult to image with MR due to susceptibility related signal loss via multiple air-tissue interfaces. Improved imaging protocols that use pulse sequences with shorter echo times,[60-63] or surface coils that provide high sensitivity in a localized region may improve sensitivity in the lungs to allow imaging of ^{19}F labeled NK cells after i.v. injection.

Concurrent with the promise of ^{19}F MRI for tracking NK cells *in vivo*, there are several remaining limitations that must be recognized and/or overcome when translating into patients. Field strengths of clinical MRI systems limit detection *in vivo* to about 10^4 cells, which may preclude detection of cells after trafficking to tumors from ancillary delivery intravenously or percutaneously. Nonetheless, optimal field strength, imaging sequence, and scan time needed to obtain sufficient SNR has not yet been fully assessed and could improve sensitivity. In addition, if the ^{19}F-labeled NK cells were to undergo cell death, macrophages or dendritic cells could phagocytose them, also leading to false positive signals. Verification of ^{19}F-labeled NK cells will therefore still need to be done pre-clinically with fluorescent or optical methods until better alternatives are available.

Methods

Animals

Female NOD.Cg-*Prkdc*^{scid}*Il2rg*^{tm1Wjl}/SzJ (NSG) mice were purchased from The Jackson Laboratory (Bar Harbor, Maine) and used between 8–16 weeks of age. All animals were bred and housed in a pathogen-free facility throughout the study. The Animal Care and Use Committee at the University of Wisconsin approved all experimental protocols.

Reagents and tumor cell lines

Peripheral blood mononuclear cells (PBMCs) and NK cells were cultured in NK media containing X-VIVO-10 (Lonza, cat#: 04-380Q) supplemented with 10% human AB serum (Corning Cellgro Inc., cat#: 35-060-Cl), 1% penicillin-strepomycin-glutamine (HyClone, cat#: SV30082.01), and 100 IU/mL recombinant human Interleukin-2 (National Cancer Institute BRB Preclinical Repository). The human chronic myelogenous leukemia cell lines K562 (American Type Culture Collection) and K562-41BBL-IL15-GFP (Waisman Biomanufacturing University of Wisconsin Madison) were maintained in RPMI-1640 (Corning Cellgro Inc., cat#: 15-040-CV) medium supplemented with 10% heat-inactivated FBS (Gibco, cat#: 10437-028) and 1% penicillin-streptomycin-glutamine (HyClone, cat#: SV30082.01) at 37°C in a humidified 5% CO_2 atmosphere. CHLA-20 human neuroblastoma was a gift from Dr Mario Otto (University of Wisconsin), initially obtained from the Children Oncology Group (COG) cell line repository. M21 human melanoma was obtained from the laboratory of Dr Paul Sondel (University of Wisconsin) and gifted by Dr Ralph Reisfeld (La Jolla, CA). Z138

human mantle cell lymphoma was purchased from the American Tissue Culture Collection. CHLA-20, M21 and Z138 cell lines were grown in RPMI-1640 medium containing 10% heat inactivated FBS and 1% penicillin-streptomycin-glutamine, as formulated above, and cultured at 37°C in a humidified 5% CO_2 atmosphere.

In vivo *tumor models and hu14.18-IL-12 immunocytokine*

Tumor cell viability was checked by trypan blue (Thermo Scientific, cat#: SV300084.01) and counted with a hemocytometer prior to *in vivo* implantation. CHLA-20, Z138 and M21 live cells at 4×10^6 were suspended in 0.1 mL PBS and injected subcutaneously into the right flanks of NSG mice. Once tumor sizes reached on average 8 × 8 cm (diameter × length), human NK cells were labeled with 4 mg/mL ^{19}F for 24 h, then extra ^{19}F was washed away from the NK cell cultures and ^{19}F-labeled NK cells were resuspended in 0.1 mL PBS and injected intratumorally at 10×10^6 or 7×10^6 cells into CHLA-20 or Z138 tumors, respectively.

For mice bearing the M21 tumors (right flank), 10×10^6 ^{19}F-labeled NK cells were resuspended in 0.1 mL PBS and injected subcutaneously in the left flank opposite to the tumor. For NSG mice bearing M21 tumors, mice were treated intraperitoneal (1×10^6 IU/0.2 mL) with recombinant human IL-2 (National Cancer Institute BRB Preclinical Repository) on days 0 and 7 and treated intratumorally (50 μg/50 μL) with hu14.18-IL2 (EMD 272063) on days 0–2 and 7–9 of ^{1}H/^{19}F imaging by MRI. The immunocytokine hu14.18-IL2 (EMD 272063), a GD2-specific monoclonal antibody (mAB) fused to human IL-2 and recognizes GD2, was gifted by Dr Paul Sondel (University of Wisconsin) and supplied by the Biological Resources NCI (Frederick, MD), EMD Pharmaceuticals (Durham, NC), Merck Serono (Darmstadt, Germany) and Apeiron Biologics (Vienna, Austria).

Isolation of NK cells

Healthy donor peripheral whole blood was obtained through an IRB-approved protocol (2012-0130-CR002). PBMCs were isolated from the buffy coats by density-gradient separation, and the lymphocyte fraction was isolated from PBMCs using Ficoll (Stem Cell Technologies, cat# 07861). For NK expansion from PBMCs, K562-41BBL-IL15 feeder cells were gamma-irradiated at 100 Gy (JL Shepherd model109 Cesium irradiator) and co-cultured with PBMCs at a 1:1 ratio of feeder cells to PBMCs in NK media. PBMCs and feeder cells were cultured at 37°C in 5% CO_2 on a shaker for 12 d. Fresh media was supplemented on days 4 and 8. On day 12, human NK cells were isolated by negative selection using magnetic cell separation beads (Miltenyi Biotec, cat#: 130-092-657) and sorted using autoMACS® Separator (Miltenyi Biotec Inc., San Diego CA). NK cell purity was determined by flow cytometry staining for anti-CD3 and anti-CD56 and purity was >95% ($CD3^-$ $CD56^+$).

^{19}F labeling and injection of NK cells

Human NK cells were cultured for 24 or 48 h in a commercially available emulsified PFPE tracer agent CS-ATM-1000 (Celsense, Pittsburgh, PA) in NK media. After 24 or 48 h, NK cells were harvested and washed three times to remove excess PFPE before *in vitro* and *in vivo* testing. NK cell viability before and after ^{19}F labeling was assayed using a standard trypan blue (Thermo Scientific, cat#: SV300084.01) exclusion method. For *in vivo* studies, ^{19}F-labeled NK cells were injected into NSG mice subcutaneously or intratumorally.

NK cell cytotoxicity

Human NK cell cytotoxic function was determined by a standard 4-h [^{51}Cr]-release assay against the NK cell–sensitive tumor cell line K562 using ^{19}F-labeled or unlabeled NK cells as effector cells. K562 cells (targets) were labeled with 50 μCi ^{51}Cr (NEZ030S; Perkin Elmer) per 10^6 cells and incubated for 60 min at 37°C, then cells were washed to remove extra ^{51}Cr and target cells were resuspended in media. K562 targets (5×10^3) were added to each well at different effector to target (E:T) ratio and incubated at 37°C for 4 h. The γ-scintillation of supernatant was measured by a γ-counter (Perkin Elmer). Maximum release was determined by adding 100 μL of 1X-Triton X-100 detergent (Sigma-Aldrich, cat#: 9002-93-1) to target cells. Spontaneous release was determined by adding 100 μL of media to 100 μL of target cells. Specific ^{51}Cr release was calculated as: % lysis = 100% × (Experimental–Spontaneous)/(Maximum–Spontaneous).

NMR

To determine labeling efficiency and quantify ^{19}F uptake by human NK cells, ^{19}F nuclear magnetic resonance (NMR) spectra were acquired on ^{19}F-labeled NK cell pellets. Human NK cells (3×10^6 or as indicated in the figure legends) were labeled with ^{19}F-PFPE (Celsense, CS-ATM-1000), pelleted to discard any ^{19}F remaining in the culture medium, and the dry cell pellets were lysed in a lysis buffer containing 1% Triton X-100 (Sigma Aldrich, cat#: 9002-93-1) and 0.1% Trifluoroacetic acid (TFA) (Sigma Aldrich, cat#: T6508) diluted in deuterium oxide (Sigma Aldrich, cat#: 7789-20-0). NK cells in lysis buffer were placed in a capillary tube. The added amount of TFA acted as both a chemical shift (−76 ppm) and quantification (three ^{19}F atoms per TFA molecule) reference for analysis. Samples were transferred into NMR vials and further diluted with D_2O such that the cell lysate solution fit the entire detection region of the NMR coil. One-dimensional (1D) ^{19}F NMR spectra were obtained on the NK cells using a 9.0 s recycle delay (TR), 90° flip angle, and 128 averages with the primary ^{19}F NMR peak from the NK cells identified around −91 ppm. All spectra were acquired using a 9.4T vertical bore Varian Unity-Inova NMR spectrometer (Agilent, Santa Clara, CA, USA). The following equation was used to determine the ^{19}F-labeling density,

$$F_c = \frac{3 \times I_s \times M_R \times N_A}{I_R \times N_c} \quad (1)$$

where F_c is the number of ^{19}F atoms per cell, I_s is the integrated area of major peak of the NK cell pellet, M_R is moles of TFA reference added, N_A is Avogardro's number, I_R is the integrated area under the TFA reference peak, and N_c is the number of

cells in pellet. The average F_c was taken as the mean from three separate samples and its uncertainty (σ_{F_c}) was estimated as the standard deviation. NMR peak integration was performed in VNMR 6.1C (Agilent, CA, USA) with plotting performed in MATLAB R2014b (The Mathworks Inc. MA, USA).

In vivo *MRI*

Prior to MRI, mice were anesthetized with 1 mg ketamine (Ketaject, NDC#: 57319-542-02) and 0.1 mg xylazine (LLOYD Inc., NADA#: 139-236) per 10 g body weight, monitored with a respiration pad, and maintained at 36°C using a warm-air blower. An external phantom vial containing PFPE with known ^{19}F spin density (ρ_R) of 2.3×10^{16} ^{19}F atoms/mm^3 was placed in the field-of-view (FOV) and used as a ^{19}F reference during image acquisition. MRI was performed on a 4.7 T small animal MRI system (Agilent Technologies, Santa Clara, CA) using a volume quadrature ^{19}F coil tunable to ^{19}F (187.9 MHz) and to ^{1}H (200 MHz). Multiple coronal ^{19}F 2 mm slice images were acquired using a multi-slice spin echo acquisition with 2000/9.0 ms TR/TE, 16 echoes, 16 kHz receiver bandwidth, 72 × 36 mm FOV, 64 × 32 matrix size, 1.1 × 1.1 mm^2 in-plane resolution, and 40 averages resulting in a 42.6 min total scan time for ^{19}F imaging. The same coil was used to acquire anatomical ^{1}H images using either a T_1-weighted gradient echo acquisition with an 80.4/3.4 ms TR/TE, 20° flip angle, and 0.28 × 0.28 mm^2 in-plane resolution or a T_2-weighted fast spin echo with a 3500/16.5 ms TR/TE, 8 echo train length and 0.28 × 0.28 mm^2 in-plane resolution. The FOV and slice thickness (2 mm) were identical for both ^{19}F and ^{1}H images to allow for easy co-registration between nuclei. One mouse bearing the human neuroblastoma CHLA-20, one mouse bearing the human mantle cell lymphoma Z138 and two mice bearing the human melanoma M21 were imaged by MRI for quantification of the number of ^{19}F-labeled NK cells and their localization *in vivo* at different time points (indicated in the figure legends for each tumor model).

Quantitative analysis of ^{19}F signal in vivo

All image analysis was performed in MATLAB R2014b (Mathworks; Natick, MA). Quantitation of the number of cells based on ^{19}F signal was performed similar to the previously published algorithm.[27] Briefly, low-SNR magnitude image voxels were corrected for their Rician distribution by generating a look-up table between measured and expected signal intensity. Using a region-of-interest (ROI) drawn in the noise/background, the standard deviation of either the real or imaginary signal of the complex ^{19}F MR data was calculated (σ_N) on a per-slice basis. This value was used to generate the look-up table and voxels with signal below a threshold of $8\times\sigma_N$ were corrected to lower signal values. Signal levels above 8 σ_N were not corrected as they approach a Gaussian distribution. Further, a minimum signal threshold of 5 σ_N was applied to select voxels with ^{19}F signal above the noise. For visualization, ^{19}F magnitude images were interpolated to match the ^{1}H image matrix size. ^{19}F images were overlaid on ^{1}H images for anatomical positioning of ^{19}F signal with the above signal threshold applied. All the voxels with ^{19}F signal above the signal threshold (S_V) were summed for all slices. The average signal in the reference vial was measured with a drawn ROI ($\bar{S}_R$). The spin density of the reference (ρ_R) was normalized to the imaging voxel size in units of ^{19}F atoms per voxel. The apparent number of cells (N_c) in the MR image could then be computed using the previously determined F_c (see Equation 1 under NMR methods) and Equation 2 below.

$$N_c = \sum (S_V) \times \frac{1}{F_c} \times \frac{\rho_R}{\bar{S}_R} \tag{2}$$

To determine the uncertainty in N_c (σ_{N_c}), Equation 3 below was used.

$$\left(\frac{\sigma_{N_c}}{N_c}\right)^2 = \left(\frac{\sigma_{S_V}}{S_V}\right)^2 + \left(\frac{\sigma_{F_c}}{F_c}\right)^2 + \left(\frac{\sigma_{\bar{S}_R}}{\bar{S}_R}\right)^2 \tag{3}$$

The uncertainty in the ^{19}F reference mean signal ($\sigma_{\bar{S}_R}$) was estimated as the standard deviation of the ROI drawn on the reference. The uncertainty in the summed ^{19}F voxel signal (σ_{S_V}) was estimated by Equation 4 below,[27]

$$\sigma_{S_V} = \sigma_N \times \sqrt{2 \times n} \tag{4}$$

where σ_N is the standard deviation of the noise in the MR image and n is the number of voxels identified as having ^{19}F signal above the noise threshold. No uncertainty was assumed in the spin density in the ^{19}F reference $\left(\sigma_{\rho_R} = 0\right)$.

Flow cytometry

Human NK cells were cultured for 24 h with different concentrations of ^{19}F PFPE or cultured without label as a control. After labeling, 1×10^6 NK cells were incubated with Fc block clone 3G8 (BD PharMingen, cat#: 564220) and stained at 4°C for 20 min with anti-human antibodies including FITC-CD3 (OKT3, cat#: 317306), PE-IgG1k (MOPC-21, cat#: 400114), PE-NKp44 (P44-8, cat#: 325108), PE-DNAM-1 (11A8, cat#: 338306), PeCy7-NKG2D (1D11, cat#: 320812), PeCy7-IgG1k (MOPC-21, cat#: 400126), PeCy7-NKp46 (9E2, cat#: 331916), AF647-NKp30 (P30-15, cat#: 325212), AF647-IgG1k (MOPC-21, cat#: 400130 and 400136), AF647-IFNγ (4S.B3, cat#: 502516), AF647-Granzyme B (GB11, cat#: 515405), APC-CX3CR1 (2A9-1, cat#: 341609), APC-CXCR4 (12G5, cat#: 306510), BV421-CD56 (HCD56, cat#: 318328), and BV510-CD45 (HI30, cat#: 304036). All antibodies were purchased from BioLegend (San Diego, CA).

For intracellular detection of IFNγ, NK cells were stimulated with media containing 1 μg/mL PMA (Sigma Aldrich, cat#: P-8139), 10 μg/mL ionomycin (Sigma Aldrich, cat#: I0634) plus Golgi Stop (BD Biosciences, cat#: 554724) and Golgi Plug (BD Biosciences, cat#: 555029) for 4 h at 37°C or in the presence of media containing only Golgi Stop and Golgi Plug. After the 4 h, cell surface staining was performed followed by intracellular staining using the BD kit Cytofix/Cytoperm Plus fixation/permeabilization kit (BD Biosciences, cat#: 555028). Flow cytometry data was acquired on a MACSQuant analyzer 10 (Miltenyi Biotec Inc., San Diego CA) and mqd files were converted to fcs files using The MACSQuantify™ Software. List-mode data were analyzed using FlowJo software (TreeStar).

ELISA

Human IFNγ levels in supernatants from unlabeled human NK cells or ^{19}F-labeled NK cells were quantified using Legend Max ELISA kit with pre-coated plates with human IFNγ according to manufacturer's instructions (BioLegend, Inc., cat#: 430107). IFNγ cytokine concentration was extrapolated relative to a standard curve created by serial dilution of human IFNγ standards run in parallel. ELISA plates were at 450 nm on a VERSAmax Tunable Plate Reader (Molecular Devices, Sunnyvale, CA) and data were collected using SOFTmax PRO software (Molecular Devices, Sunnyvale, CA).

Statistical analysis

Statistics were performed using GraphPad Prism version 6.0 for the Macintosh OS (GraphPad Software, San Diego, CA). Data were expressed as mean ± SEM. For analysis of three or more groups, the non-parametric ANOVA test was performed with the Bonferroni or Sidak's multiple comparisons post-test. Analysis of differences between two normally distributed test groups was performed using the Student's t-test. Welch's correction was applied to Student's t-test data sets with significant differences in variance. A p value less than 0.05 was considered statistically significant.

Disclosure of potential conflicts of interest

No potential conflicts of interest were disclosed.

Acknowledgments

We would like to thank Michael Martinez, Mallery Olsen, Erbay Salievski, and Lauren Reil for valuable assistance with this study. Thank you to Beth Rauch and the Department of Medical Physics for core scan time to allow methods development and to the University of Wisconsin Carbone Comprehensive Cancer Center (UWCCC) Flow Cytometry core. Stand Up To Cancer is a program of the Entertainment Industry Foundation administered by the American Association for Cancer Research. The content is solely the responsibility of the authors and does not necessarily represent the official views of the National Institutes of Health.

Funding

This work is supported in part by the UWCCC, NIH/NCI K08 CA174750, NIH/NCATS UL1TR000427 and TL1TR000429, the Stand Up To Cancer – St. Baldrick's Pediatric Dream Team Translational Research Grant SU2C-AACR-DT1113 (C.M.C.), NCI P30 CA014520 – UWCCC (B.B., S.B.F. and C.M.C.), American Cancer Society (B.B., S.B.F. and C.M.C.), Alex's Lemonade Stand Foundation (C.M.C.), The American Association of Immunologists Careers in Immunology Fellowship (M.N.B) and the St. Baldrick's Foundation (M.P.K. and C.M.C).

References

1. Arai S, Meagher R, Swearingen M, Myint H, Rich E, Martinson J, Klingemann H. Infusion of the allogeneic cell line NK-92 in patients with advanced renal cell cancer or melanoma: a phase I trial. Cytotherapy 2008; 10:625-32; PMID:18836917; http://dx.doi.org/10.1080/14653240802301872
2. deMagalhaes-Silverman M, Donnenberg A, Lembersky B, Elder E, Lister J, Rybka W, Whiteside T, Ball E. Posttransplant adoptive immunotherapy with activated natural killer cells in patients with metastatic breast cancer. J Immunother 2000; 23:154-60; PMID:10687148; http://dx.doi.org/10.1097/00002371-200001000-00018
3. Geller MA, Cooley S, Judson PL, Ghebre R, Carson LF, Argenta PA, Jonson AL, Panoskaltsis-Mortari A, Curtsinger J, McKenna D et al. A phase II study of allogeneic natural killer cell therapy to treat patients with recurrent ovarian and breast cancer. Cytotherapy 2011; 13:98-107; PMID:20849361; http://dx.doi.org/10.3109/14653249.2010.515582
4. Lister J, Rybka WB, Donnenberg AD, deMagalhaes-Silverman M, Pincus SM, Bloom EJ, Elder EM, Ball ED, Whiteside TL. Autologous peripheral blood stem cell transplantation and adoptive immunotherapy with activated natural killer cells in the immediate posttransplant period. Clin Cancer Res 1995; 1:607-14; PMID:9816022
5. Miller JS, Soignier Y, Panoskaltsis-Mortari A, McNearney SA, Yun GH, Fautsch SK, McKenna D, Le C, Defor TE, Burns LJ et al. Successful adoptive transfer and in vivo expansion of human haploidentical NK cells in patients with cancer. Blood. 2005 Apr 15; 105(8):3051-; PMID:15632206; http://dx.doi.org/10.1182/blood-2004-07-2974
6. Tonn T, Schwabe D, Klingemann HG, Becker S, Esser R, Koehl U, Suttorp M, Seifried E, Ottmann OG, Bug G. Treatment of patients with advanced cancer with the natural killer cell line NK-92. Cytotherapy 2013; 15:1563-70; PMID:24094496; http://dx.doi.org/10.1016/j.jcyt.2013.06.017
7. Minutes. Meeting #45. Food and Drug Administration Center for Biologics Evaluation and Research April 10 and 11, 2008; Cell, Tissue and Gene Therapies Advisory Committee.
8. Jha P, Golovko D, Bains S, Hostetter D, Meier R, Wendland MF, Daldrup-Link HE. Monitoring of natural killer cell immunotherapy using noninvasive imaging modalities. Cancer Res 2010; 70:6109-13; PMID:20631071; http://dx.doi.org/10.1158/0008-5472.CAN-09-3774
9. Sta Maria NS, Barnes SR, Jacobs RE. In vivo monitoring of natural killer cell trafficking during tumor immunotherapy. Magn Reson Insights 2014; 7:15-21; PMID:25114550; http://dx.doi.org/10.4137/MRI.S13145
10. Daldrup-Link HE, Meier R, Rudelius M, Piontek G, Piert M, Metz S, Settles M, Uherek C, Wels W, Schlegel J et al. In vivo tracking of genetically engineered, anti-HER2/neu directed natural killer cells to HER2/neu positive mammary tumors with magnetic resonance imaging. Eur Radiol 2005; 15:4-13; PMID:15616814; http://dx.doi.org/10.1007/s00330-004-2526-7
11. Mallett CL, McFadden C, Chen Y, Foster PJ. Migration of iron-labeled KHYG-1 natural killer cells to subcutaneous tumors in nude mice, as detected by magnetic resonance imaging. Cytotherapy 2012; 14:743-51; PMID:22443465; http://dx.doi.org/10.3109/14653249.2012.667874
12. Meier R, Golovko D, Tavri S, Henning TD, Knopp C, Piontek G, Rudelius M, Heinrich P, Wels WS, Daldrup-Link, H. Depicting adoptive immunotherapy for prostate cancer in an animal model with magnetic resonance imaging. Magn Reson Med: Off J Soc Magnet Resonance Med / Soc Magnet Resonance Med 2011; 65:756-63; PMID:20928869; http://dx.doi.org/10.1002/mrm.22652
13. Sheu AY, Zhang Z, Omary RA, Larson AC. MRI-monitored transcatheter intra-arterial delivery of SPIO-labeled natural killer cells to hepatocellular carcinoma: preclinical studies in a rodent model. Invest Radiol 2013; 48:492-9; PMID:23249649; http://dx.doi.org/10.1097/RLI.0b013e31827994e5
14. Ahrens ET, Flores R, Xu H, Morel PA. In vivo imaging platform for tracking immunotherapeutic cells. Nat Biotechnol 2005; 23:983-7; PMID:16041364; http://dx.doi.org/10.1038/nbt1121
15. Ruiz-Cabello J, Barnett BP, Bottomley PA, Bulte JW. Fluorine (19F) MRS and MRI in biomedicine. NMR Biomed 2011; 24:114-29; PMID:20842758; http://dx.doi.org/10.1002/nbm.1570
16. Grégoire C, Cognet C, Chasson L, Coupet C-A, Dalod M, Reboldi A, Marvel J, Sallusto F, Vivier E, Walzer T. Intrasplenic trafficking of natural killer cells is redirected by chemokines upon inflammation. Euro J Immunol 2008; 38:2076-84; PMID:18624307; http://dx.doi.org/10.1002/eji.200838550
17. Liou HLR, Myers JT, Barkauskas DS, Huang AY. Intravital imaging of the mouse popliteal lymph node. 2012:e3720. J Vis Exp. 2012 Feb 8; (60). pii: 3720. PMID: 22349264; http://dx.doi.org/10.3791/3720

18. Olson JA, Zeiser R, Beilhack A, Goldman JJ, Negrin RS. Tissue-specific homing and expansion of donor NK cells in allogeneic one marrow transplantation. J Immunol 2009; 183:3219-28; PMID:19657090; http://dx.doi.org/10.4049/jimmunol.0804268
19. F.D.A. US. White paper: initiative to reduce unnecessary radiation exposure from medical imaging.
20. Ahrens ET, Bulte JW. Tracking immune cells in vivo using magnetic resonance imaging. Nat Rev Immunol 2013; 13:755-63; PMID:24013185; http://dx.doi.org/10.1038/nri3531
21. Ahrens ET, Zhong J. In vivo MRI cell tracking using perfluorocarbon probes and fluorine-19 detection. NMR Biomed 2013; 26:860-71; PMID:23606473; http://dx.doi.org/10.1002/nbm.2948
22. Hu L, Hockett FD, Chen J, Zhang L, Caruthers SD, Lanza GM, Wickline SA. A generalized strategy for designing (19)F/(1)H dual-frequency MRI coil for small animal imaging at 4.7 Tesla. J Magn Reson Imaging: JMRI 2011; 34:245-52; PMID:21698714; http://dx.doi.org/10.1002/jmri.22516
23. Lim YT, Cho MY, Noh YW, Chung JW, Chung BH. Near-infrared emitting fluorescent nanocrystals-labeled natural killer cells as a platform technology for the optical imaging of immunotherapeutic cells-based cancer therapy. Nanotechnology 2009; 20:475102; PMID:19875875; http://dx.doi.org/10.1088/0957-4484/20/47/475102
24. Hitchens TK, Ye Q, Eytan DF, Janjic JM, Ahrens ET, Ho C. 19F MRI detection of acute allograft rejection with in vivo perfluorocarbon labeling of immune cells. Magn Reson Med: Off J Soc Magn Reson Med / Soc Magn Reson Med 2011; 65:1144-53; PMID:21305593; http://dx.doi.org/10.1002/mrm.22702
25. Helfer BM, Balducci A, Nelson AD, Janjic JM, Gil RR, Kalinski P, de Vries IJ, Ahrens ET, Mailliard RB. Functional assessment of human dendritic cells labeled for in vivo (19)F magnetic resonance imaging cell tracking. Cytotherapy 2010; 12:238-50; PMID:20053146; http://dx.doi.org/10.3109/14653240903446902
26. Bonetto F, Srinivas M, Heerschap A, Mailliard R, Ahrens ET, Figdor CG, de Vries IJ. A novel (19)F agent for detection and quantification of human dendritic cells using magnetic resonance imaging. Int J Cancer J Int du Cancer 2011; 129:365-73; PMID:20839261; http://dx.doi.org/10.1002/ijc.25672
27. Srinivas M, Morel PA, Ernst LA, Laidlaw DH, Ahrens ET. Fluorine-19 MRI for visualization and quantification of cell migration in a diabetes model. Magn Reson Med: Off J Soc Mag Reson Med / Soc Magn Reson Med 2007; 58:725-34; PMID:17899609; http://dx.doi.org/10.1002/mrm.21352
28. Srinivas M, Turner MS, Janjic JM, Morel PA, Laidlaw DH, Ahrens ET. In vivo cytometry of antigen-specific t cells using 19F MRI. Magn Reson Med: Off J Soc Magn Reson Med / Soc Magn Reson Med 2009; 62:747-53; PMID:19585593; http://dx.doi.org/10.1002/mrm.22063
29. Helfer BM, Balducci A, Sadeghi Z, O'Hanlon C, Hijaz A, Flask CA, Wesa A. (1)(9)F MRI tracer preserves in vitro and in vivo properties of hematopoietic stem cells. Cell Transplant 2013; 22:87-97; PMID:22862925; http://dx.doi.org/10.3727/096368912X653174
30. Ruiz-Cabello J, Walczak P, Kedziorek DA, Chacko VP, Schmieder AH, Wickline SA, Lanza GM, Bulte JW. In vivo "hot spot" MR imaging of neural stem cells using fluorinated nanoparticles. Magn Reson Med: Off J Soc Magn Reson Med/ Soc Magn Reson Med 2008; 60:1506-11; PMID:19025893; http://dx.doi.org/10.1002/mrm.21783
31. Boehm-Sturm P, Mengler L, Wecker S, Hoehn M, Kallur T. In vivo tracking of human neural stem cells with 19F magnetic resonance imaging. PloS One 2011; 6:e29040; PMID:22216163; http://dx.doi.org/10.1371/journal.pone.0029040
32. Gaudet JM, Ribot EJ, Chen Y, Gilbert KM, Foster PJ. Tracking the fate of stem cell implants with fluorine-19 MRI. PloS One 2015; 10:e0118544; PMID:25767871; http://dx.doi.org/10.1371/journal.pone.0118544
33. Ribot EJ, Gaudet JM, Chen Y, Gilbert KM, Foster PJ. In vivo MR detection of fluorine-labeled human MSC using the bSSFP sequence. Int J Nanomed 2014; 9:1731-9; PMID:24748787; http://dx.doi.org/10.2147/IJN.S59127
34. Ahrens ET, Helfer BM, O'Hanlon CF, Schirda C. Clinical cell therapy imaging using a perfluorocarbon tracer and fluorine-19 MRI. Magn Reson Med: Off J Soc Magn Reson Med / Soc Magn Reson Med 2014; 72:1696-701; PMID:25241945; http://dx.doi.org/10.1002/mrm.25454
35. Lim YT, Cho MY, Kang JH, Noh YW, Cho JH, Hong KS, Chung JW, Chung BH. Perfluorodecalin/[InGaP/ZnS quantum dots] nanoemulsions as 19F MR/optical imaging nanoprobes for the labeling of phagocytic and nonphagocytic immune cells. Biomaterials 2010; 31:4964-71; PMID:20346494; http://dx.doi.org/10.1016/j.biomaterials.2010.02.065
36. Gilfillan S, Chan CJ, Cella M, Haynes NM, Rapaport AS, Boles KS, Andrews DM, Smyth MJ, Colonna M. DNAM-1 promotes activation of cytotoxic lymphocytes by nonprofessional antigen-presenting cells and tumors. J Exp Med 2008; 205:2965-73; PMID:19029380; http://dx.doi.org/10.1084/jem.20081752
37. Buhtoiarov IN, Neal ZC, Gan J, Buhtoiarova TN, Patankar MS, Gubbels JA, Hank JA, Yamane B, Rakhmilevich AL, Reisfeld RA et al. Differential internalization of hu14.18-IL2 immunocytokine by NK and tumor cell: impact on conjugation, cytotoxicity, and targeting. J Leukocyte Biol 2011; 89:625-38; PMID:21248148; http://dx.doi.org/10.1189/jlb.0710422
38. Neal ZC, Yang JC, Rakhmilevich AL, Buhtoiarov IN, Lum HE, Imboden M, Hank JA, Lode HN, Reisfeld RA, Gillies SD et al. Enhanced activity of hu14.18-IL2 immunocytokine against murine NXS2 neuroblastoma when combined with interleukin 2 therapy. Clin Cancer Res: Off J Am Assoc Cancer Res 2004; 10:4839-47; PMID:15269160; http://dx.doi.org/10.1158/1078-0432.CCR-03-0799
39. Lode HN, Xiang R, Dreier T, Varki NM, Gillies SD, Reisfeld RA. Natural killer cell-mediated eradication of neuroblastoma metastases to bone marrow by targeted interleukin-2 therapy. Blood 1998; 91:1706-15; PMID:9473237
40. Yang RK, Kalogriopoulos NA, Rakhmilevich AL, Ranheim EA, Seo S, Kim K, Alderson KL, Gan J, Reisfeld RA, Gillies SD et al. Intratumoral treatment of smaller mouse neuroblastoma tumors with a recombinant protein consisting of IL-2 linked to the hu14.18 antibody increases intratumoral CD8+ T and NK cells and improves survival. Cancer Immunol, Immunother: CII 2013; 62:1303-13; PMID:23661160; http://dx.doi.org/10.1007/s00262-013-1430-x
41. Shusterman S, London WB, Gillies SD, Hank JA, Voss SD, Seeger RC, Reynolds CP, Kimball J, Albertini MR, Wagner B et al. Antitumor activity of hu14.18-IL2 in patients with relapsed/refractory neuroblastoma: a Children's Oncology Group (COG) phase II study. J Clin Oncol: Off J Am Soc Clin Oncol 2010; 28:4969-75; PMID:20921469; http://dx.doi.org/10.1200/JCO.2009.27.8861
42. Osenga KL, Hank JA, Albertini MR, Gan J, Sternberg AG, Eickhoff J, Seeger RC, Matthay KK, Reynolds CP, Twist C et al. A phase I clinical trial of the hu14.18-IL2 (EMD 273063) as a treatment for children with refractory or recurrent neuroblastoma and melanoma: a study of the Children's Oncology Group. Clin Cancer Res: Off J Am Assoc Cancer Res 2006; 12:1750-9; PMID:16551859; http://dx.doi.org/10.1158/1078-0432.CCR-05-2000
43. Albertini MR, Hank JA, Gadbaw B, Kostlevy J, Haldeman J, Schalch H, Gan J, Kim K, Eickhoff J, Gillies SD et al. Phase II trial of hu14.18-IL2 for patients with metastatic melanoma. Cancer Immunol, Immunother: CII 2012; 61:2261-71; PMID:22678096; http://dx.doi.org/10.1007/s00262-012-1286-5
44. Cheng M, Chen Y, Xiao W, Sun R, Tian Z. NK cell-based immunotherapy for malignant diseases. Cell Mol Immunol 2013; 10:230-52; PMID:23604045; http://dx.doi.org/10.1038/cmi.2013.10
45. Spahn DR. Blood substitutes. Artificial oxygen carriers: perfluorocarbon emulsions. Crit Care 1999; 3:R93-7; PMID:11094488; http://dx.doi.org/10.1186/cc364
46. Bansal A, Pandey MK, Demirhan YE, Nesbitt JJ, Crespo-Diaz RJ, Terzic A, Behfar A, DeGrado TR. Novel (89)Zr cell labeling approach for PET-based cell trafficking studies. EJNMMI Res 2015; 5:19; PMID:25918673; http://dx.doi.org/10.1186/s13550-015-0098-y
47. van de Watering FC, Rijpkema M, Perk L, Brinkmann U, Oyen WJ, Boerman OC. Zirconium-89 labeled antibodies: a new tool for molecular imaging in cancer patients. Biomed Res Int 2014; 2014:203601; PMID:24991539; http://dx.doi.org/10.1155/2014/203601
48. Sato N, Wu H, Asiedu KO, Szajek LP, Griffiths GL, Choyke PL. (89)Zr-oxine complex PET cell imaging in monitoring cell-based therapies. Radiology 2015; 275:490-500; PMID:25706654; http://dx.doi.org/10.1148/radiol.15142849

49. Brand JM, Meller B, Von Hof K, Luhm J, Bahre M, Kirchner H, Frohn C. Kinetics and organ distribution of allogeneic natural killer lymphocytes transfused into patients suffering from renal cell carcinoma. Stem Cells Dev 2004; 13:307-14; PMID:15186726; http://dx.doi.org/10.1089/154732804323099235
50. Meller B, Frohn C, Brand JM, Lauer I, Schelper LF, von Hof K, Kirchner H, Richter E, Baehre M. Monitoring of a new approach of immunotherapy with allogenic (111)In-labelled NK cells in patients with renal cell carcinoma. Euro J Nuclear Med Mol Imaging 2004; 31:403-7; PMID:14685783; http://dx.doi.org/10.1007/s00259-003-1398-4
51. Matera L, Galetto A, Bello M, Baiocco C, Chiappino I, Castellano G, Stacchini A, Satolli MA, Mele M, Sandrucci S et al. In vivo migration of labeled autologous natural killer cells to liver metastases in patients with colon carcinoma. J Transl Med 2006; 4:49; PMID:17105663; http://dx.doi.org/10.1186/1479-5876-4-49
52. Kircher MF, Gambhir SS, Grimm J. Noninvasive cell-tracking methods. Nat Rev Clin Oncol 2011; 8:677-88; PMID:21946842; http://dx.doi.org/10.1038/nrclinonc.2011.141
53. Tavri S, Jha P, Meier R, Henning TD, Muller T, Hostetter D, Knopp C, Johansson M, Reinhart V, Boddington S et al. Optical imaging of cellular immunotherapy against prostate cancer. Mol Imaging 2009; 8:15-26; PMID:19344572; http://dx.doi.org/10.2310/7290.2009.00002
54. Jang ES, Shin JH, Ren G, Park MJ, Cheng K, Chen X, Wu JC, Sunwoo JB, Cheng Z. The manipulation of natural killer cells to target tumor sites using magnetic nanoparticles. Biomaterials 2012; 33:5584-92; PMID:22575830; http://dx.doi.org/10.1016/j.biomaterials.2012.04.041
55. Olson JA, Zeiser R, Beilhack A, Goldman JJ, Negrin RS. Tissue-specific homing and expansion of donor NK cells in allogeneic bone marrow transplantation. J Immunol 2009; 183:3219-28; PMID:25241945; http://dx.doi.org/10.4049/jimmunol.0804268
56. Beuneu H, Deguine J, Breart B, Mandelboim O, Di Santo JP, Bousso P. Dynamic behavior of NK cells during activation in lymph nodes. Blood 2009; 114:3227-34; PMID:19667398; http://dx.doi.org/10.1182/blood-2009-06-228759
57. Sutton EJ, Henning TD, Pichler BJ, Bremer C, Daldrup-Link HE. Cell tracking with optical imaging. Eur Radiol 2008; 18:2021-32; PMID:18506449; http://dx.doi.org/10.1007/s00330-008-0984-z
58. Duval L, Schmidt H, Kaltoft K, Fode K, Jensen JJ, Sorensen SM, Nishimura MI, von der Maase H. Adoptive transfer of allogeneic cytotoxic T lymphocytes equipped with a HLA-A2 restricted MART-1 T-cell receptor: a phase I trial in metastatic melanoma. Clin Cancer Res: Off J Am Assoc Cancer Res 2006; 12:1229-36; PMID:16489078; http://dx.doi.org/10.1158/1078-0432.CCR-05-1485
59. Hasumi K, Aoki Y, Wantanabe R, Mann DL. Clinical response of advanced cancer patients to cellular immunotherapy and intensity-modulated radiation therapy. Oncoimmunology 2013; 2:e26381; PMID:24349874; http://dx.doi.org/10.4161/onci.26381
60. Schmid F, Holtke C, Parker D, Faber C. Boosting (19) F MRI-SNR efficient detection of paramagnetic contrast agents using ultrafast sequences. Magn Reson Med: Off J Soc Magn Reson Med / Soc Magn Reson Med 2013; 69:1056-62; PMID:19657090; http://dx.doi.org/10.1002/mrm.24341
61. Johnson KM, Fain SB, Schiebler ML, Nagle S. Optimized 3D ultrashort echo time pulmonary MRI. Magn Reson Med: Off J Soc Magn Reson Med / Soc Magn Reson Med 2013; 70:1241-50; PMID:23213020; http://dx.doi.org/10.1002/mrm.24570
62. Weiger M, Pruessmann KP, Hennel F. MRI with zero echo time: hard versus sweep pulse excitation. Magn Reson Med: Off J Soc Magn Reson Med / Soc Magn Reson Med 2011; 66:379-89; PMID:21381099; http://dx.doi.org/10.1002/mrm.22799
63. Grodzki DM, Jakob PM, Heismann B. Ultrashort echo time imaging using pointwise encoding time reduction with radial acquisition (PETRA). Magn Reson Med: Off J Soc Magn Reson Med / Soc Magn Reson Med 2012; 67:510-8; http://dx.doi.org/10.1002/mrm.23017